SOIL, 11, 85–94, 2025
https://doi.org/10.5194/soil-11-85-2025

SOIL Open Access EGU

Effect of colloidal particle size on physicochemical properties and aggregation behaviors of two alkaline soils

Yuyang Yan[1], Xinran Zhang[1], Chenyang Xu[1,2], Junjun Liu[1], Feinan Hu[3,4], and Zengchao Geng[1,2]

[1]College of Natural Resources and Environment, Northwest A&F University, Yangling, Shaanxi 712100, China
[2]Key Laboratory of Plant Nutrition and the Agri-Environment in Northwest China, Ministry of Agriculture, Northwest A&F University, Yangling, Shaanxi 712100, China
[3]State Key Laboratory of Soil Erosion and Dryland Farming on the Loess Plateau, Northwest A&F University, Yangling, Shaanxi 712100, China
[4]Institute of Soil and Water Conservation, Chinese Academy of Sciences, Ministry of Water Resources, Yangling, Shaanxi 712100, China

Correspondence: Chenyang Xu (xuchenyang@nwafu.edu.cn, xuchenyang.ms@163.com)

Received: 29 April 2024 – Discussion started: 11 June 2024
Revised: 29 October 2024 – Accepted: 11 November 2024 – Published: 27 January 2025

Abstract. Colloidal particles are the most active soil components, and they vary in elemental composition and environmental behaviors with the particle size due to the heterogeneous nature of natural soils. The purposes of the present study are to clarify how particle size affects the physicochemical properties and aggregation kinetics of soil colloids and to further reveal the underlying mechanisms. Soil colloidal fractions, from two alkaline soils – Anthrosol and Calcisol – were subdivided into three ranges: $d < 2\,\mu m$, $d < 1\,\mu m$ and $d < 100\,nm$. The organic and inorganic carbon contents, clay mineralogy and surface electrochemical properties, including surface functional groups and zeta potentials, were characterized. Through a time-resolved light scattering technique, the aggregation kinetics of soil colloidal fractions were investigated, and their critical coagulation concentrations (CCCs) were determined. With decreasing colloidal particle diameter, the total carbon content, organic carbon, organic functional groups' content and illite content all increased. The zeta potential became less negative, and the charge variability decreased with decreasing particle diameter. The CCC values of Anthrosol and Calcisol colloids followed the descending order of $d < 100\,nm$, $d < 1\,\mu m$ and $d < 2\,\mu m$. Compared with the course factions ($d < 1$ and $d < 2\,\mu m$), soil nanoparticles were more abundant in organic carbon and more stable clay minerals ($d < 100\,nm$); thus they exhibited strongest colloidal suspension stability. The differences in organic matter contents and clay mineralogy are the fundamental reasons for the differences in colloidal suspension stability behind the size effects of Anthrosol and Calcisol colloids. The present study revealed the size effects of two alkaline soil colloids on carbon content, clay minerals, surface properties and suspension stability, emphasizing that soil nanoparticles are prone to be more stably dispersed instead of being aggregated. These findings can provide references for in-depth understanding of the environmental behaviors of the heterogeneous soil organic–mineral complexes.

Published by Copernicus Publications on behalf of the European Geosciences Union.

1 Introduction

Soils contain a series of solid particles in continuous sizes, ranging over 6 orders of magnitude from nanometers to millimeters (Lead and Wilkinson, 2006; Li et al., 2011), among which soil colloids are the most reactive fractions. Soil colloids are characterized by high surface area and abundant surface charges, exhibiting high potential for carbon sequestration and strong adsorption capacity, which can largely determine the fate and transport of pathogens, nutrients, heavy metals and organic pollutants and might cause environmental problems to adjacent water bodies or groundwater (Baalousha, 2009; Calabi-Floody et al., 2011). Due to their high reactivity and fluidity in aqueous environment, soil colloids play an important role in physical, chemical and biogeochemical processes in natural environments (Schäfer et al., 2012; Mayordomo et al., 2016). The capacity of soil colloids in mobilizing bound nutrients and pollutants is closely related to their dispersion stability under various environmental conditions (Won and Burns, 2018). Therefore, studies on the dispersion stability of soil colloids have attracted extensive attention.

Currently, the definition of soil and environmental colloidal fractions is ambiguous. Soil colloidal fractions are defined as soil particles with diameters of $< 1\,\mu m$ (Lead and Wilkinson, 2006; Weil and Brady, 2016) and also diameters of $< 2\,\mu m$ (Zhang et al., 2021), while in some extreme cases, they can refer to particles with diameters of 5–10 µm (Yin et al., 2010). Such discrepancies are seen among publications due to the fact that colloids are defined based on the particle diameter range within which they can display colloidal properties. Since for different materials, e.g., metal (Fe/Al/Ti) oxides, silica gel and phyllosilicates, the specific colloidal range differs greatly.

Compared with engineered nanoparticles with known mineralogical organization, natural soils are much more heterogeneous (Cárdenas et al., 2010); their elemental composition and clay mineralogy of soil colloids change with particle size. Tsao et al. (2013) found that quartz and feldspar were mainly dominant in colloidal particles of $< 2\,\mu m$ and 450–2000 nm in red soil (Ferralsols, WRB, IUSS Working Group WRB, 2022), while illite and montmorillonite were the main clay minerals in nanoparticles (1–100 nm). In addition, the mineral structure at nanometer scale also changes. Compared with colloidal particles of $< 2\,\mu m$, the Si/Al ratio in nanoparticles increased, and the surface area, morphology, crystallinity, surface atomic structure and frame structure were significantly different (Tsao et al., 2011). Furthermore, particle size also affects the surface potential of soil colloids. Tang et al. (2015) investigated the surface potential variations with particle size (1–10 µm, 0.5–1 µm, 0.2–0.5 µm, $< 0.2\,\mu m$) for variably charged yellow soil (Lixisols) and permanently charged purple soil (Leptosols); among the colloidal fractions, the absolute surface potential of the finest particles of purple soil (Leptosols) was lowest, while that of the yellow soil (Lixisols) was the largest, caused by the differences in surface charge density. Thus, the influences of particle size on elemental composition and surface properties of soils should be further studied.

In recent years, great progress has been made in the study of dispersion stability of soil clay minerals, such as montmorillonite, kaolinite, illite or hematite, and soil nanoparticles (Xu et al., 2018; Sun et al., 2020; Wei et al., 2021; Zhu et al., 2014). He et al. (2008) demonstrated that hematite nanoparticles with various particle diameters showed different surface properties and aggregation behaviors under the same pH conditions; moreover, the critical coagulation concentrations (CCCs) of hematite decreased with the decrease in particle diameter. Zhou et al. (2013) compared the CCCs of 10 different TiO_2 nanoparticles with varying sizes and indicated that crystal structure and particle diameter both affected the aggregation behaviors of TiO_2. Zhang et al. (2016) confirmed that the types of clay minerals for two Alfisols changed from smectite and vermiculite to kaolinite and illite when the particle size varied from colloids to nanoparticles. Therefore, the dependence of physicochemical properties, surface properties and environmental behaviors on particle size for heterogeneous soil colloidal particles needs systematic investigation.

In the present study, soil colloidal particles of two alkaline soils – Anthrosols and Calcisols – were subdivided into three ranges: $d < 2\,\mu m$, $d < 1\,\mu m$ and $d < 100\,nm$. Their organic fraction, clay mineralogy, surface electrochemical properties and colloidal stability were studied. This study selected two representative calcareous soils to verify the following scientific hypothesis: soil colloids are organic–inorganic composites. As particle diameter decreases (from colloid particles to nanoparticles), the number of organic functional groups on the surface of soil colloids increases, and the type of clay minerals shifts towards finer clay particles, e.g., illite, resulting in increased specific surface area and decreased charge density, and thus enhanced suspension stability, meaning particle diameter influences the composition of soil colloidal fractions, thereby changing surface properties and suspension stability. The findings can have important implications for predicting the environmental performances of colloids and colloid-facilitated nutrients, polluters and pathogens in the natural soil and water environment.

2 Materials and methods

2.1 Soil sampling

The study collected two surface soil samples (0–20 cm), Lou soil and Cinnamon soil, the most common and characteristic calcareous soils, by mixing soils from 5–10 sampling points using a stainless-steel auger in Yangling District (38°18′14″ N, 108°2′30″ E) and in Zhouzhi County (34°8′8″ N, 108°3′10″ E), on the Guanzhong Plain, Shaanxi Province, northwest China. Among these, Lou soil, as a

unique calcareous soil, has formed on the basis of Cinnamon soil through long-term anthropogenic maturation. According to the World Reference Base for Soil Resources (WRB, IUSS Working Group WRB, 2022), Lou soil and Cinnamon soil are classified as Hortic Endoanthric Anthrosols (Loamic, Luvic, Eutric, Calcic) and Calcic Protocalcic Calcisols (Loamic, Lixic, Humic), respectively. Both types of soil are developed from loess parent material. The typical soil profile configuration for the tested Anthrosols is Ap1-Ap2-Bt-Bk-C, while for the Calcisols, it is Ah-Bt-Bk-C.

Soils samples were taken back to the laboratory for air-drying and sieving. The basic soil properties were determined based on standard methods. Soil pH was measured with a pH electrode, employing a solution-to-soil ratio of 2.5 : 1. Soil organic carbon (SOC) was determined using the $K_2Cr_2O_7$ oxidation method. The cation exchange capacity (CEC) of soil was measured with an exchange method. The $CaCO_3$ content was determined by a gasometric method. The free Fe/Al oxides were extracted by dithionite-citrate-bicarbonate (DCB) solution. The particle size distribution was measured using the Malvern Mastersizer 2000 laser diffractometer (Malvern Instruments Ltd., UK). The pH of Anthrosols was 8.34, while it was 8.32 for Calcisols. The SOCs of Anthrosols and Calcisols were 7.25 and 9.22 g kg^{-1}, respectively. The CECs of Anthrosols and Calcisols were 25.9 and 22.2 cmol kg^{-1}. The contents of $CaCO_3$ in Anthrosols and Calcisols were 51.7 and 82.5 g kg^{-1}. The free Fe/Al oxide contents of Anthrosols and Calcisols were 22.8 and 23.1 g kg^{-1}. The proportions of sand (2–0.02 mm), silt (0.02–0.002 mm) and clay (< 0.002 mm) in Anthrosols were 34.0 %, 40.6 % and 25.4 %, while they were 28.0 %, 44.8 % and 27.2 % for the Calcisols.

2.2 Extraction of soil colloidal fractions in different size ranges

The soil colloidal particles were extracted based on Stokes' law, and detailed procedures can be found in our previous publication (Hu et al., 2022). Briefly, 50 g of dry soil was weighed in a beaker containing 500 mL of distilled water, and the suspension was put under sonication for an hour using an ultrasonic cell disrupter (XO-900D, Nanjing Xianou Instruments Corporation, China) while maintaining the temperature below 30 °C. Afterwards, the suspension was transferred to a larger beaker, and distilled water was added to make up the total volume of 5 L. The suspension was further dispersed using an electronic blade stirrer (JB-200, Shanghai Nanhui Huiming Apparatus, China) for 1 h, before being sieved through a sieve with a pore size of 53 µm, and the upper suspensions containing soil colloidal particles in different diameters were collected by centrifugation. Based on Eq. (1), centrifugation speed and time for colloidal particles of $d < 2$ µm, < 1 µm and < 100 nm were calculated, and they are shown in Table S1.

$$t = \frac{\eta \lg \frac{R_2}{R_1}}{3.81 N^2 r^2 \Delta d}, \quad (1)$$

where t is time for centrifugation (s); R_1 is the distance from the surface of the liquid to the center of the axis of the centrifuge, which is 5.7 cm here; R_2 is the distance from the particles to the center of the axis of the centrifuge, which is 10.5 cm here; N (rev s^{-1}) is the centrifuge speed; r (cm) is the desired colloidal particle radius; Δd is the difference in density between the soil particles (2.65 g cm^{-3}) and water (1 g cm^{-3}), while Δd is 1.65 g cm^{-3}; and η is the water viscosity coefficient, which is 0.00839 g cm^{-1} s^{-1} at 25 °C here.

2.3 Characterization of soil colloidal fractions in different size ranges

The initial particle diameters of soil colloids were determined by a time-resolved dynamic light scattering (DLS) apparatus (Nanobrook Omni, Brookhaven, USA). Each sample was measured 15 times to get the initial particle diameters. The organic carbon contents in soil colloids were determined by a potassium dichromate external heating method, and total carbon content was determined by an elemental analyzer (Elementar Vario EL III, Germany). Total carbon and organic carbon are the averaged results of three measurements each. The inorganic carbon content was calculated by a subtraction method (Wang et al., 2011). The clay mineralogy of soil colloids was determined by X-ray diffraction (XRD; Ultima-IV, Rigaku, Japan), and by comparing the intensity of the dominant XRD peak of the soil mineral colloid to a standard mineral reference (Database ICDD 2004), the relative percentage content of the minerals was determined. The specific surface areas of the soil colloids were measured by the BET-N_2 method (ASAP 2460, Micromeritics Instrument, USA). High-resolution spectra of C1s and O1s of soil colloids were acquired by X-ray photoelectron spectroscopy (XPS) (Thermo Scientific K-Alpha, USA) (Luo et al., 2019), and the Gaussian–Lorentzian curve-fitting program (XPSPEAK 4.1) was used to analyze the XPS spectra. The zeta potentials of soil colloids were measured by Zeta PALS equipped with the BI-ZTU Autotitrator (ZetaPALS, Brookhaven, USA) with a 1 mmol L^{-1} NaCl solution as the background electrolyte, and the pH range of colloidal suspension was set to 3–10, adjusted with 0.1 mol L^{-1} HCl and NaOH. Each sample was measured six times to get the average zeta potential values. The concentrations of K^+, Na^+, Ca^{2+} and Mg^{2+} in soil colloidal suspensions were measured using flame atomic absorption spectrophotometry (PinAAcle 900F, USA).

2.4 Aggregation kinetics of soil colloidal fractions

The aggregation kinetic curves of soil colloidal particles in different electrolytes were determined by time-resolved DLS measurements. The incident wavelength was 635 nm, and the scattering angle was 90°. The stock colloidal suspensions with particle concentration of 200 mg L^{-1} were mixed with electrolyte solutions with equal volume. The suspension pH was adjusted to 8.0, which was close to the pH value of natural soil with an addition of 0.1 mol L^{-1} HCl or NaOH before measurement. The chosen electrolyte concentrations for NaCl and $CaCl_2$ were 200–2000 and 2–20 mmol L^{-1}. The effective diameter (D_h) of the mixed sample was automatically recorded every 2 min, and an aggregation kinetic curve was obtained in 30 min monitoring. According to the method generally adopted by most research, the aggregation curve was determined only one time without repetition (Chen and Elimelech, 2006; Mashayekhi et al., 2012; Zhu et al., 2014; Liu et al., 2018).

2.5 Calculation of critical coagulation concentration

According to particle interaction theory, the aggregation kinetic curves under electrolyte conditions can be divided into a reaction-limited aggregation (RLA) stage under low concentration, which was affected by electrolyte conditions, and a diffusion-limited aggregation (DLA) stage under high concentration, which was not affected by electrolyte concentration. The CCC is the critical electrolyte concentration when the aggregation process changes from the RLA state ($\alpha < 1$) to the DLA state ($\alpha = 1$). Attachment efficiency (α) represents the bonding probability of particle collisions and can be calculated for each electrolyte concentration using Eq. (2), which allowed the curve of α to be plotted as a function of electrolyte concentration (Xu et al., 2020a; Hu et al., 2022).

$$\alpha_{exp} = \frac{1}{W} = \frac{k_{11}}{(k_{11})_{fast}} = \frac{\frac{1}{N_0}\left(\frac{da_h(t)}{d_t}\right)_{t\to 0}}{\frac{1}{(N_0)_{fast}}\left(\frac{da_h(t)}{d_t}\right)_{t\to 0,fast}}, \quad (2)$$

where D_h is the effective diameter of particles, t is the time (min), N_0 is the density of particles, K_{11} is the aggregation rate of RLA and $(K_{11})_{fast}$ is the aggregation rate of DLA. The intersection of the RLA regime and DLA regime is the CCC.

The aggregation rates were calculated by the average of the last five effective diameters divided by the aggregation time at a specific electrolyte concentration. The fractal dimension in the DLA regime was obtained based on the method proposed by Wang et al. (2013).

$$D(t) = b \cdot t^n + D_0, \quad (3)$$

where $D(t)$ is the colloidal effective diameter at time t (min), D_0 is the initial effective diameter of colloids, and b and n are constants determined by the aggregation curves. The fractal dimension is $d_f = 1/n$ in the DLA regime.

3 Results and discussion

3.1 Particle size and distribution characteristics of Anthrosol and Calcisol colloidal fractions

The average diameters of Anthrosol and Calcisol colloids were measured by time-resolved DLS, and the results are shown in Table 1. The number-weighted diameters for Anthrosol colloids of $d < 2$ µm were about 1.04 times of $d < 1$ µm and about 1.84 times of $d < 100$ nm, respectively. The intensity-weighted diameters for Anthrosol colloids were 294.10–396.81 nm. For Calcisol colloidal fractions, the number-weighted diameters for colloids of $d < 2$ µm were about 1.07 times of $d < 1$ µm and about 1.65 times of $d < 100$ nm, and the intensity-weighted diameters were 312.25–439.20 nm. The intensity-weighted diameters were generally higher than the number-weighted diameters, especially in polydisperse system (Xu et al., 2020b). The colloidal particles in the soil solution were in constant Brownian motion; upon illumination by light, these colloidal particles scatter light, causing variations in light intensity. This phenomenon allowed for the calculation of the effective diameter of the particles, which was the intensity-weighted diameter (Filella et al., 1997). Considering that the particle diameter is proportional to the sixth power of light intensity, the number-weighted diameter typically provided a more accurate representation of the true diameter of colloidal particles in polydisperse systems containing larger particles (Xu et al., 2015).

From Table 1, it can be seen that the average colloidal diameters of $d < 2$ µm were close to the diameter of $d < 1$ µm, and they were both significantly higher than the diameter of the nano-sized fraction. From the particle size distribution characteristics, it is clear that the size range indicated by the differences of D_{90} and D_{10} increased with intended particle diameter. For Anthrosol and Calcisol, 74.69 % and 63.55 % of all particles contained in the colloidal suspensions of $d < 100$ nm were actually less than 100 nm, respectively, indicating the complexity of soil colloidal particle irregularity.

3.2 Physicochemical properties and clay mineralogy of Anthrosol and Calcisol colloids

Table 2 shows the physicochemical properties of soil colloidal fractions. The yields of each colloidal fraction of Anthrosol were slightly larger than that of Calcisol, respectively. The yields of colloidal particles of $d < 2$ µm were about 1.3–1.4 times of $d < 1$ µm and about 4.0–4.9 times of $d < 100$ nm, respectively. With the decreasing colloidal particle diameter, the total carbon content, organic carbon and inorganic carbon content all increased, suggesting the finer particles were richer in carbon. This tendency is in agreement with other publications (Zhang et al., 2021; Said-Pullicino et al., 2021; Hu et al., 2022). The specific surface areas for colloidal fractions of $d < 1$ µm were largest of all, which may be

Table 1. The average diameters and distribution patterns of soil colloids.

Soil type	Colloidal fractions	Number-weighted diameter (nm)	Intensity-weighted diameter (nm)	D_{10} (nm)	D_{90} (nm)
Anthrosol	$d < 2\,\mu m$	133.16 ± 24.28	396.81 ± 12.34	71.53	232.49
	$d < 1\,\mu m$	127.84 ± 20.29	371.45 ± 11.88	67.64	219.87
	$d < 100\,nm$	72.47 ± 7.04	294.10 ± 15.80	38.74	136.72
Calcisol	$d < 2\,\mu m$	141.23 ± 24.33	439.20 ± 12.72	78.29	244.97
	$d < 1\,\mu m$	131.67 ± 15.77	372.07 ± 8.23	75.84	231.64
	$d < 100\,nm$	85.48 ± 16.93	312.25 ± 33.58	47.84	158.99

Note that D_{10}, D_{50} and D_{90} represent the diameter of particles with a cumulative distribution of 10 %, 50 % and 90 %, respectively.

related to the structures of formed clusters while drying the samples for observation under microscopy (Yu et al., 2017; Weissenberger et al., 2021). Furthermore, Anthrosol and Calcisol nanoparticles exhibited the lowest specific surface area. This phenomenon arose from organic substances adsorbing relatively little inorganic nitrogen (Li et al., 2013; Wilson et al., 2008). Therefore, however, to our knowledge, no other better method has been reported for measuring the specific surface area of natural nanoparticles.

The clay mineralogy of Anthrosol and Calcisol colloidal fractions is shown in Table 3. Calcisol colloidal fractions were dominant by illite, kaolinite and chlorite, while there was less chlorite in Anthrosol colloidal fractions. With the decrease in particle size, the content of illite increased and kaolinite content decreased. This tendency is in agreement with other publications (Chenu and Plante, 2006; Zhang et al., 2016). Among the dominant clay types, the size of illite is finer than kaolinite and chlorite (Weil and Brady, 2016), so its mass percentage was higher in the nano-sized fraction.

3.3 Surface properties of Anthrosol and Calcisol colloids

The XPS spectra of soil colloidal fractions are shown in Fig. 1. From Fig. 1, it can be seen that the main C-containing functional groups were C–C/C–H/C=C, C–O, C=O and COO– groups at 284.6, 286.2, 288.0 and 289.4 eV, respectively (Liang et al., 2020; Ding et al., 2023). The functional groups for colloidal particles of $d < 100\,nm$ were more abundant than those for colloids of $d < 2$ and $d < 1\,\mu m$, while there were no significant differences between colloids of $d < 2$ and $d < 1\,\mu m$. With the decrease in colloidal particle diameter, the relative contents of oxygen-containing functional groups (C–O, C=O, COO–) gradually decreased. Specifically, the content decreased gradually from 32.01 % in Lou colloids of $d < 2\,\mu m$ to 20.93 % in Lou colloids of $d < 100\,nm$ (Table S2 in the Supplement). The functional groups of C–O and COO– gradually decreased until they eventually disappeared; more C=O groups were exposed to the surrounding air.

For Calcisol colloids (Fig. 1d, e, f), the relative contents of organic oxygen-containing functional groups for colloidal

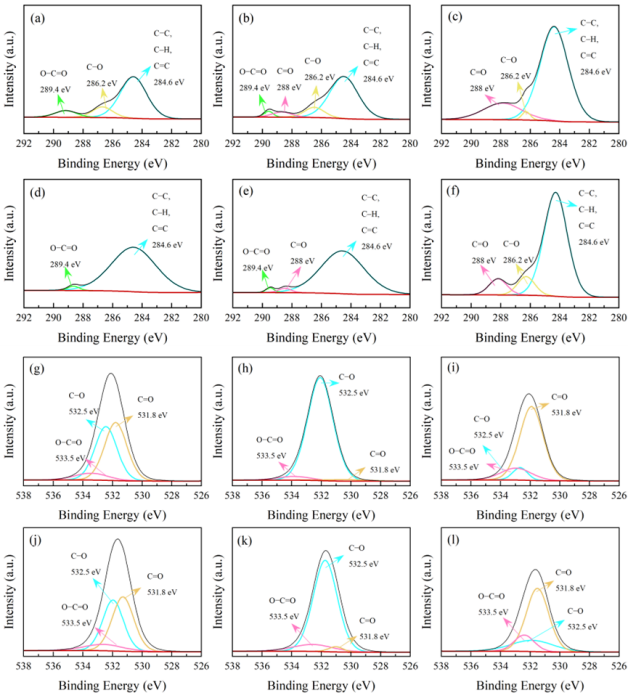

Figure 1. The photoelectron spectrum C1s and O1s peak diagram of Anthrosol and Calcisol colloids. C1s of Anthrosol colloids, **(a)** $d < 2\,\mu m$, **(b)** $d < 1\,\mu m$ and **(c)** $d < 100\,nm$; C1s of Calcisol colloids, **(d)** $d < 2\,\mu m$, **(e)** $d < 1\,\mu m$ and **(f)** $d < 100\,nm$; O1s of Anthrosol colloids, **(g)** $d < 2\,\mu m$, **(h)** $d < 1\,\mu m$ and **(i)** $d < 100\,nm$; O1s of Calcisol colloids, **(j)** $d < 2\,\mu m$, **(k)** $d < 1\,\mu m$ and **(l)** $d < 100\,nm$.

particles of $d < 2\,\mu m$, $d < 1\,\mu m$ and $d < 100\,nm$ showed a different trend, compared with that in Anthrosol colloids. The relative contents of organic oxygen-containing functional groups gradually increased with the decrease in diameter. This trend was particularly pronounced in fractions of $d < 100\,nm$, and the contents of C–O and COO– were highly increased (Table S2).

Oxygen-containing functional groups of C–O, C=O and COO– are electronegative functional groups; hydroxyl and carboxyl groups can lose protons and make the surface of

Table 2. The physicochemical properties of soil colloids.

Soil type	Colloidal fractions	Yield (%)	Total carbon content ($g\,kg^{-1}$)	Organic carbon content ($g\,kg^{-1}$)	$CaCO_3$ content ($g\,kg^{-1}$)	Specific surface area ($m^2\,g^{-1}$)
Anthrosol	$d < 2\,\mu m$	25.12	20.90 ± 0.30	10.90 ± 1.29	10.00	65.37
	$d < 1\,\mu m$	18.76	20.65 ± 0.15	10.91 ± 0.43	9.74	72.99
	$d < 100\,nm$	6.32	58.25 ± 0.35	27.38 ± 0.21	30.87	45.28
Calcisol	$d < 2\,\mu m$	23.17	24.00 ± 0.30	11.66 ± 0.60	12.34	49.99
	$d < 1\,\mu m$	16.20	22.30 ± 0.20	12.76 ± 0.11	9.54	61.88
	$d < 100\,nm$	4.70	76.30 ± 0.40	28.31 ± 0.15	47.99	34.53

Table 3. The dominant clay minerals of soil colloidal fractions (shown in mass fraction, %).

Soil type	Colloidal fractions	Illite	Kaolinite	Chlorite	Vermiculite
Anthrosol	$d < 2\,\mu m$	34	23	4	9
	$d < 1\,\mu m$	30	22	7	11
	$d < 100\,nm$	37	14	16	3
Calcisol	$d < 2\,\mu m$	24	22	29	16
	$d < 1\,\mu m$	31	19	25	12
	$d < 100\,nm$	37	16	17	5

soil colloidal particles carry negative charges (Audette et al., 2021). Functional groups of C–O, C = O and COO– can affect the negative charges carried on the colloidal surface by forming hydrogen bonds, and their polarity can also affect the negative charges on the surface when the O atom combines with C and H. The electrons will lean towards the O atom with stronger electronegativity, which also makes the colloidal surface carry negative charges (Tan et al., 2019). The contents and types of oxygen-containing functional groups are one of the main factors affecting colloid charge and aggregation.

The zeta potential values of different colloidal fractions in the pH range of 3–10 are shown in Fig. 2. Zeta potentials of the colloidal particles were negative, indicating that they were negatively charged. The zeta potentials of Anthrosol and Calcisol colloidal particles were more negative with increasing solution pH, due to the deprotonation of the surface (Moayedi and Kazemian, 2013; Dong et al., 2019). Compared with the Calcisol colloids, the zeta potentials of Anthrosol colloidal particles were more negative, due to Anthrosol possessing a higher surface charge density. For Calcisol colloids, the differences among colloidal fractions were larger.

In general, zeta potential became more negative with increasing particle diameter. When the pH changed from 3 to 10, for every pH unit increase, the zeta potential values of Anthrosol colloids of $d < 2\,\mu m$, $< 1\,\mu m$ and $< 100\,nm$ would be increased by 2.14, 2.09 and 1.89 mV; and for Calcisol colloids, these variation rates were 2.15, 1.45 and 1.37 mV, respectively. These data demonstrate that the charge variability decreases with decreasing particle diameter. Song et al. (2019) compared the zeta potential of wheat straw biochar nanoparticles ($< 100\,nm$) and colloidal particles ($< 1000\,nm$) and found that the absolute values of colloidal particles were larger at the same pH, which was explained by the differences in the number of surface carboxyl and hydroxyl groups. The zeta potential of colloidal particles is proportional to charge density, which means that it is related to both charge quantity and specific surface area (Hou et al., 2009). Therefore, the size effect of zeta potential of Anthrosol and Calcisol colloidal particles is mainly related to the reduction of charge density caused by a larger specific surface area of nanoparticles (Xu et al., 2020b).

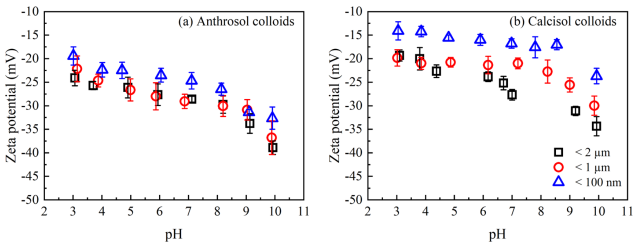

Figure 2. The zeta potential of Anthrosol **(a)** and Calcisol **(b)** colloids of $d < 2\,\mu m$, $< 1\,\mu m$ and $< 100\,nm$ at different pH.

3.4 Aggregation kinetics curves of Anthrosol and Calcisol colloids in NaCl and $CaCl_2$ solutions

The aggregation kinetics of Anthrosol and Calcisol colloids in NaCl and $CaCl_2$ solutions are shown in Figs. S1 and S2 in the Supplement. The aggregation process of soil colloids was divided into RLA and DLA stages. The RLA stages for Anthrosol colloids of $d < 2\,\mu m$, $d < 1\,\mu m$ and $d < 100\,nm$ in the NaCl solution were 0–80, 0–80 and 0–100 mmol L^{-1}, respectively, during which repulsive forces existed between the particles, and attachment did not occur for every collision. As the electrolyte concentration continued to increase, the solution entered into the DLA regime. At this point, attachment occurred with every collision between particles, and the aggregation rates were not affected by the electrolyte concentration. At last, the effective diameters of the formed clusters were stable at around 1600 nm. Figure S1b, d and f showed that the aggregation behaviors of Anthrosol colloids in $CaCl_2$ solution were similar to those in the NaCl solution, and the corresponding $CaCl_2$ concentrations for Anthrosol colloids of $d < 2\,\mu m$, $d < 1\,\mu m$ and $d < 100\,nm$ in the RLA stage were about 0–1.5, 0–1.5 and 0–2 mmol L^{-1}, respectively.

The aggregation kinetics of Calcisol colloids in NaCl and $CaCl_2$ solutions were similar to Anthrosol colloids (Fig. S2). The RLA stages for Calcisol colloids of $d < 2\,\mu m$, $d < 1\,\mu m$ and $d < 100\,nm$ in the NaCl solution were 0–100, 0–120 and 0–250 mmol L^{-1} and were about 0–1.8, 0–1.7 and 0–2 mmol L^{-1} in the $CaCl_2$ solution, respectively. The effective diameters of the clusters for Calcisol colloids were stabilized at about 1600 and 1800 nm in NaCl and $CaCl_2$ solutions, respectively.

Aggregation rates of soil colloids varied with particle diameter at the same electrolyte concentration, which was particularly evident in RLA stage (Table 4). With decreasing particle diameter, the aggregation rates of Anthrosol and Calcisol colloids in 50 mmol L^{-1} NaCl and 1 mmol L^{-1} $CaCl_2$ solutions exhibited a corresponding decline. In addition, in 50 mmol L^{-1} NaCl solution, the aggregation rates for Anthrosol colloids of $d < 2\,\mu m$, $d < 1\,\mu m$ and $d < 100\,nm$ were about 2.17, 2.09 and 1.95 times those of Calcisol colloids, while the aggregation rates were about 1.46, 1.57 and 1.91 times those of Calcisol colloids in 1 mmol L^{-1} $CaCl_2$ solution, respectively. Therefore, from Table 4, the aggregation rates of Anthrosol and Calcisol colloids showed the size effect. From Table 4, it could be observed that the fractal dimensions in NaCl solutions were largely higher than those in $CaCl_2$ solutions, suggesting a much denser structure (Meng et al., 2013). In other words, the formed structures in divalent solutions were more open.

3.5 Suspension stability of Anthrosol and Calcisol colloids in NaCl and $CaCl_2$ solutions

The CCCs for Anthrosol colloids of $d < 2\,\mu m$, $d < 1\,\mu m$ and $d < 100\,nm$ in the NaCl solution were 80.40, 91.78 and 134.96 mmol L^{-1}, respectively (Fig. 3a), and those for Calcisol colloids were 121.10, 126.50 and 292.86 mmol L^{-1}, respectively (Fig. 3b). The CCCs increased with decreasing particle diameter, indicating that the suspension stability of soil nanoparticles was stronger than that of colloidal particles.

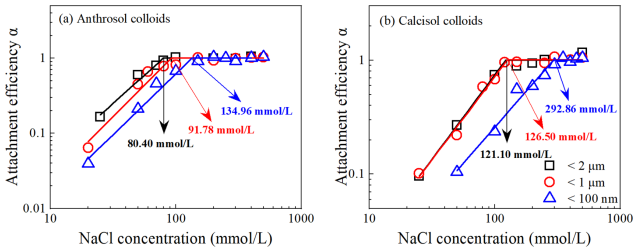

Figure 3. The CCCs of Anthrosol **(a)** and Calcisol **(b)** colloids of $d < 2\,\mu m$, $< 1\,\mu m$ and $< 100\,nm$ in the NaCl solution.

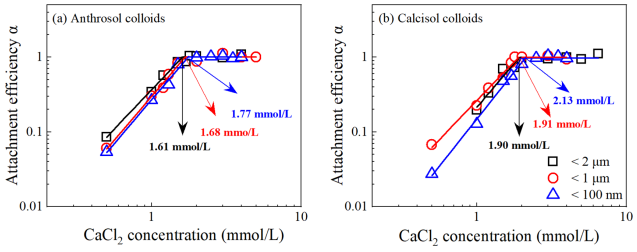

Figure 4. The CCC of Anthrosol **(a)** and Calcisol **(b)** colloids of $d < 2\,\mu m$, $< 1\,\mu m$ and $< 100\,nm$ in the $CaCl_2$ solution.

In $CaCl_2$ solutions, the CCCs for Anthrosol colloids of $d < 2\,\mu m$, $d < 1\,\mu m$ and $d < 100\,nm$ were 1.61, 1.68 and 1.77 mmol L^{-1}, respectively, and for Calcisol colloids, those corresponding values were 1.90, 1.91 and 2.13 mmol L^{-1} (Fig. 4). The CCCs in $CaCl_2$ solutions also increased with decreasing particle size. The contents of K^+, Na^+, Ca^{2+} and Mg^{2+} in Anthrosol and Calcisol colloidal suspensions decreased with the decreasing colloidal particle diameter (Table S3), which was mainly due to the dilution effect during the extraction process. Furthermore, Table S3 shows that the soluble cation contents were rather low, and their effects on the CCCs of soil colloids could be neglected.

Based on Figs. 3 and 4, the 3 mmol L^{-1} $CaCl_2$ solution could cause fast aggregation of soil colloidal particles, while it required at least a 80 mmol L^{-1} NaCl solution for a comparable aggregation rate, indicating that the shielding effect of divalent cations on negative charges of colloids was stronger than that of monovalent cations. The quantitative calculation results showed that the CCC ratios of monovalent ion and divalent ion system were between 25.64 and 27.09, which conformed to the Schulze–Hardy rule (Baalousha, 2017).

For each type of the soil colloids, the higher the absolute zeta potential values of colloidal particles, the more negative charges carried on the surface, and the higher the stability (CCCs) of suspension. For the same particle diameter,

Table 4. The aggregation rates of soil colloids.

Soil type	Colloidal fractions	Aggregation rate		Fractal dimension	
		In 50 mmol L^{-1} NaCl (nm min^{-1})	In 1 mmol L^{-1} $CaCl_2$ (nm min^{-1})	Na	Ca
Anthrosol	$d < 2\,\mu m$	19.46	12.01	1.69 ± 0.19	1.33 ± 0.26
	$d < 1\,\mu m$	14.91	11.48	1.75 ± 0.06	1.52 ± 0.19
	$d < 100\,nm$	7.72	9.97	1.71 ± 0.26	1.68 ± 0.13
Calcisol	$d < 2\,\mu m$	8.98	8.22	1.30 ± 0.17	1.36 ± 0.17
	$d < 1\,\mu m$	7.15	7.33	1.71 ± 0.24	1.30 ± 0.31
	$d < 100\,nm$	3.95	5.22	1.52 ± 0.22	1.58 ± 0.19

e.g., $d < 100$ nm, the absolute zeta potentials of Anthrosol colloids were larger (Fig. 2), while the corresponding CCC was lower (Figs. 3 and 4). Study on the stability of biochar nanoparticles showed that the absolute values of zeta potentials could not be used to directly explain the stability difference among biochar nanoparticles from different feedstock materials but could explain the influences of solution conditions on the stability of biochar nanoparticles derived from the same feedstock material (Xu et al., 2020a).

The CCCs of Anthrosol and Calcisol colloids increased with decreasing diameter; that is, the CCCs of Anthrosol and Calcisol colloids both showed the size effects. Hsu and Kuo (1995) demonstrated that the CCCs would generally decrease with increasing particle diameter because smaller particles possess thicker double electric layers and higher electrolyte concentration is needed to neutralize charges on the surface. This was consistent with the results of Anthrosol and Calcisol colloids. The above explanation by Hsu and Kuo (1995) was derived from homogeneous particles, whose composition does not change with particle diameter. The results of this paper show that, for the two alkaline soils that are heterogeneous in nature, when the organic matter contents and mineral types changed with colloidal particle diameter, the CCCs in monovalent and divalent solutions also decreased with increasing particle diameter.

In this paper, the organic matter contents of soil nanoparticles were the highest, so the CCCs were the largest, which were 1.7 and 2.4 times of the corresponding colloidal particles of $d < 2\,\mu m$. The suspension stability of different clay minerals has been reported to vary with the mineralogical structure. The CCC of illite (≈ 100 mM) in NaCl solution was significantly higher than that of kaolinite (≈ 20 mM) (Jiang et al., 2012; Xu et al., 2017), indicating that the stability of illite suspensions is significantly higher than that of kaolinite. Therefore, another possible reason for the higher stability of soil nanoparticles is the increase in illite content and the decrease in kaolinite content. Therefore, the differences in organic matter contents and clay mineralogy are the fundamental reasons for the differences in colloidal suspension stability behind the size effects of Anthrosol and Calcisol colloids.

4 Conclusions

This study obtained soil colloidal fractions with three different particle sizes from Anthrosol and Calcisol using high-speed centrifugation and revealed the particle size effects on the soil constituents, surface properties and aggregation behavior of heterogeneous soil colloids. The results showed that, compared to coarse colloids ($d < 2\,\mu m$ and $d < 1\,\mu m$), the organic carbon contents of Anthrosol and Calcisol nanoparticles were higher, at 27.38 and 28.31 g kg^{-1}, respectively, approximately 2 and 3 times higher than those of the coarse colloids and the bulk soils, indicating that nanoparticles exhibit a strong potential for carbon sequestration. The absolute zeta potential values of soil nanoparticles decreased with decreasing average particle diameter, indicating a reduction in charge density. Anthrosol and Calcisol nanoparticles exhibited greater suspension stability in NaCl and $CaCl_2$ solutions. On the one hand, this was due to the increased thickness of the double electric layer on the surface of soil nanoparticles, resulting in stronger repulsive forces between particles; on the other hand, it was due to the presence of more illite, which has a higher CCC compared to other clay minerals. In conclusion, for such a highly heterogeneous system as soil, the size effects on soil colloidal suspension stability are strongly influenced by variations driven essentially by mineral composition. Future studies should further explore the mechanisms underlying the size effects of the typical soils on particle interactions, coagulation and transport behaviors under environmentally relevant conditions.

Data availability. https://data.mendeley.com/preview/vy7hnt3fth?a=988aaf9b-1d2a-484e-bb2d-c568d4558e9d, Digital Commons Data, 2025

Supplement. The supplement related to this article is available online at: https://doi.org/10.5194/soil-11-85-2025-supplement.

Author contributions. Conceptualization, CYX, ZCG and FNH; methodology, CYX; software, YYY; formal analysis, JJL; investigation, XRZ; resources, YYY; writing (original draft), YYY; writing (review and editing), CYX and FNH; visualization, CYX and YYY; funding acquisition, CYX, ZCG and FNH. All authors have read and agreed to the published version of the paper.

Competing interests. The contact author has declared that none of the authors has any competing interests.

Disclaimer. Publisher's note: Copernicus Publications remains neutral with regard to jurisdictional claims made in the text, published maps, institutional affiliations, or any other geographical representation in this paper. While Copernicus Publications makes every effort to include appropriate place names, the final responsibility lies with the authors.

Financial support. This work was supported by the Natural Science Foundation of Shaanxi Province (grant no. 2023-JC-YB-263), the National Natural Science Foundation of China (grant no. 41701261) and the Fundamental Research Funds for the Central Universities (grant no. 2452020165).

Review statement. This paper was edited by Karsten Kalbitz and reviewed by two anonymous referees.

References

Audette, Y., Congreves, K. A., Schneider, K., Zaro, G. C., Nunes, A. L. P., Nunes, A. L. P., Zhang, H. J., and Voroney, R. P.: The effect of agroecosystem management on the distribution of C functional groups in soil organic matter: A review, Biol. Fertil. Soils, 57, 881–894, 2021.

Baalousha, M.: Aggregation and disaggregation of iron oxide nanoparticles: Influence of particle concentration, pH and natural organic matter, Sci. Total Environ., 407, 2093–2101, 2009.

Baalousha, M.: Effect of nanomaterial and media physicochemical properties on nanomaterial aggregation kinetics, Nano Impact, 6, 55–68, 2017.

Calabi-Floody, M., Bendall, J. S., Jara, A. A., Welland, M. E., Theng, B. K. G., Rumpel, C., and Mora, M. L.: Nanoclays from an Andisol: Extraction, properties and carbon stabilization, Geoderma, 161, 159–167, https://doi.org/10.1016/j.geoderma.2010.12.013, 2011.

Cárdenas, J. P., Santiago, A., Tarquis, A. M., Losada, J. C., Borondo, F., and Benito, R. M.: Soil porous system as heterogeneous complex network, Geoderma, 160, 13–21, 2010.

Chen, K. L. and Elimelech, M.: Aggregation and deposition kinetics of Fullerene (C_{60}) nanoparticles, Langmuir, 22, 10994–11001, 2006.

Chenu, C. and Plante, A. F.: Clay-sized organo-mineral complexes in a cultivation chronosequence: revisiting the concept of the "primary organo-mineral complex", Eur. J. Soil Sci., 57, 596–607, 2006.

Digital Commons Data: Elsevier, Welcome Homepage, Elsevier, https://data.mendeley.com/preview/vy7hnt3fth?a=988aaf9b-1d2a-484e-bb2d-c568d4558e9d, (last access: 21 January 2025), 2025.

Ding, W., Liang, H. X., Zhang, H. W., Sun, H., Geng, Z. C., and Xu, C. Y.: A cellulose/bentonite grafted polyacrylic acid hydrogel for highly-efficient removal of Cd(II), J. Water Process. Eng., 51, 103414, https://doi.org/10.1016/j.jwpe.2022.103414, 2023.

Dong, S. N., Zeng, Z., Cai, W. W., Zhou, Z. Y., Dou, C. B., Liu, H., and Xia, J. H.: The zeta potentials of g-C_3N_4 nanoparticles: Effect of electrolyte, ionic strength, pH, and humic acid, J. Nanopart Res., 21, 233, https://doi.org/10.1007/s11051-019-4686-z, 2019.

Filella, M., Zhang, J. W., Newman, M. E., and Buffle, J.: Analytical applications of photon correlation spectroscopy for size distribution measurements of natural colloidal suspensions: capabilities and limitations, Colloid Surf. A., 120, 27–46, 1997.

He, Y. T., Wan, J., and Tokunaga, T.: Kinetic stability of hematite nanoparticles, The effect of particle sizes, J. Nanopart Res., 10, 321–332, 2008.

Hou, J., Li, H., Zhu, H. L., and Wu, L. S.: Determination of clay surface potential, a more reliable approach, Soil Sci. Soc. Am. J., 73, 1658–1663, 2009.

Hsu, J. P. and Kuo, Y. C.: An Extension of the Schulze-Hardy Rule to Asymmetric Electrolytes, J. Colloid Interface Sci., 171, 254–255, 1995.

Hu, N., Xu, C. Y., Geng, Z. C., Hu, F. N., Li, Q. R., Ma, R. T., and Wang, Q.: The interplay of particle properties and solution chemistry on aggregation kinetics of soil nanoparticles, J. Soils Sediments, 22, 1761–1772, 2022.

IUSS Working Group WRB: World Reference Base for Soil Resources. International soil classification system for naming soils and creating legends for soil maps, 4th Edn., International Union of Soil Sciences (IUSS), Vienna, Austria, 2022.

Jiang, C. L., Séquaris, J. M., Vereecken, H., and Klumpp, E.: Effects of inorganic and organic anions on the stability of illite and quartz soil colloids in Na-, Ca- and mixed Na-Ca systems, Colloids Surf. A, 415, 134–141, 2012.

Lead, J. R. and Wilkinson, K. J.: Aquatic Colloids and Nanoparticles: Current Knowledge and Future Trends, Environ. Chem., 3, 159–171, 2006.

Li, S. X., Luo, Y. M., Zhang, H. B., Huang, Y. J., Li, Z., and Wei, J.: Arsenic forms in various particle-size fractions of red soil-Chemical fractionation and speciation using XANES analysis, Acta Sci. Circumst., 31, 2733–2739, 2011.

Li, W. Y., Zhu, X. Y., He, Y., Xing, B. S., and Xu, J. M.: Enhancement of water solubility and mobility of phenanthrene by natural soil nanoparticles, Environ Pollut., 176, 228–233, 2013.

Liang, H. X., Sun, R. R., Song, B., Sun, Q. Q., Peng, P., and She, D.: Preparation of nitrogen-doped porous carbon material by a hydrothermal-activation two-step method and its high-efficiency adsorption of Cr(VI), J. Hazard. Mater., 387, 121987, 2020.

Liu, G., Zheng, H., Jiang, Z., Zhao, J., Wang, Z., Pan, B., and Xing, B.: Formation and physicochemical characteristics of nano biochar: insight into chemical and colloidal stability, Environ. Sci. Technol., 52, 10369–10379, 2018.

Luo, J. J., Niu, Q., Jin, M. C., Cao, Y. A., Ye, L. R., and Du, R. P.: Study on the effects of oxygen-containing functional groups on

Hg^0 adsorption in simulated flue gas by XAFS and XPS analysis, J. Hazard. Mater., 376, 21–28, 2019.

Mashayekhi, H., Ghosh, S., Du, P., and Xing, B.: Effect of natural organic matter on aggregation behavior of C60 fullerene in water, J. Colloid Interf. Sci., 374, 111–117, 2012.

Mayordomo, N., Degueldre, C., Alonso, U., and Missana, T.: Size distribution of FEBEX bentonite colloids upon fast disaggregation in low-ionic strength water, Clay Miner., 51, 213–222, 2016.

Meng, Z. Y., Hashmi, S. M., and Elimelech, M.: Aggregation rate and fractal dimension of fullerene nanoparticles via simultaneous multiangle static and dynamic light scattering measurement, J. Colloid Interface Sci., 392, 27–33, 2013.

Moayedi, H. and Kazemian, S.: Zeta potentials of suspended humus in multivalent cationic saline solution and its effect on electro-osomosis behavior, J. Dispers Sci. Technol., 34, 283–294, 2013.

Said-Pullicino, D., Giannetta, B., Demeglio, B., Missong, A., Gottselig, N., Romani, M., Bol, R., Klumpp, E., and Celi, L.: Redox-driven changes in water-dispersible colloids and their role in carbon cycling in hydromorphic soils, Geoderma, 385, 114894, https://doi.org/10.1016/j.geoderma.2020.114894, 2021.

Schäfer, T., Huber, F., Seher, H., Missana, T., Alonso, U., Kumke, M., Eidner, S., Claret, F., and Enzmann, F.: Nanoparticles and their influence on radionuclide mobility in deep geological formations, Appl. Geochemistry., 27, 390–403, 2012.

Song, B. Q., Chen, M., Zhao, L., Qiu, H., and Cao, X. D.: Physicochemical property and colloidal stability of micron- and nanoparticle biochar derived from a variety of feedstock sources, Sci. Total Environ., 661, 685–695, 2019.

Sun, Y. L., Pan, D. Q., Wei, X. Y., Xian, D. F., Wang, P., and Hou, J. J.: Insight into the stability and correlated transport of kaolinite colloid: Effect of pH, electrolytes and humic substances, Environ. Pollut., 266, 115189, https://doi.org/10.1016/j.envpol.2020.115189, 2020.

Tan, Z. X., Yuan, S. N., Hong, M. F., Zhang, L. M., and Huang, Q. Y.: Mechanism of negative surface charge formation on biochar and its effect on the fixation of soil Cd, J. Hazard. Mater., 384, 121370, https://doi.org/10.1016/j.jhazmat.2019.121370, 2019.

Tang, Y., Li, H., Liu, X. M., Zhu, H. L., and Tian, R.: Unraveling the size distributions of surface properties for purple soil and yellow soil, J. Environ. Sci. (China), 32, 81–89, 2015.

Tsao, T. M., Chen, Y. M., Sheu, H., Tzou, Y. M., Chou, Y. M., and Wang, M. K.: Separation and identification of soil nanoparticles by conventional and synchrotron X-ray diffraction, Appl. Clay Sci., 85, 1–7, 2013.

Tsao, T. M., Chen, Y. M., Wang, M. K., and Huang, P. M.: Structural transformation and physicochemical properties of environmental nanoparticles by comparison of various particle-size fractions, Soil Sci. Soc. Am. J., 75, 533–541, 2011.

Wang, L. F., Wang, L. L., Ye, X. D., Li, W. W., Ren, X. M., Sheng, G. P., Yu, H. Q., and Wang, X. K.: Coagulation kinetics of humic aggregates in mono-and di-valent electrolyte solutions, Environ. Sci. Technol., 47, 5042–5049, https://doi.org/10.1021/es304993j, 2013.

Wang, Q. R., Li, Y. C., and Wang, Y.: Optimizing the weight loss-on-ignition methodology to quantify organic and carbonate carbon of sediments from diverse sources, Environ. Monit. Assess., 174, 241–257, 2011.

Wei, X. Y., Pan, D. Q., Xu, Z., Xian, D. F., Li, X. L., Tan, Z. Y., Liu, C. L., and Wu, W. S.: Colloidal stability and correlated migration of illite in the aquatic environment: The roles of pH, temperature, multiple cations and humic acid, Sci. Total Environ., 768, 144174, https://doi.org/10.1016/j.scitotenv.2020.144174, 2021.

Weil, R. R. and Brady, N. C.: The Nature and Properties of Soils, Global Edition, Pearson Education Limited, 2016.

Weissenberger, G., Henderikx, R. J., and Peters, P. J.: Understanding the invisible hands of sample preparation for cryo-EM, Nat. Methods., 18, 463–471, 2021.

Wilson, M. A., Tran, N. H., Milev, A. S., Kannangara, G. S. K., and Volk, H.: Nanomaterials in soils, Geoderma, 146, 291–302, 2008.

Won, J. and Burns, S. E.: Role of Immobile Kaolinite Colloids in the Transport of Heavy Metals, Environ. Sci. Technol., 52, 2735–2741, 2018.

Xu, C. Y., Deng, K. Y., Li, J. Y., and Xu, R. K.: Impact of environmental conditions on aggregation kinetics of hematite and goethite nanoparticles, J. Nanopart Res., 17, 394, https://doi.org/10.1007/s11051-015-3198-8, 2015.

Xu, C. Y., Li, Q. R., Geng, Z. C., Hu, F. N., and Zhao, S. W.: Surface properties and suspension stability of low–temperature pyrolyzed biochar nanoparticles: Effects of solution chemistry and feedstock sources, Chemosphere, 259, 127510, https://doi.org/10.1016/j.chemosphere.2020.127510, 2020a.

Xu, C. Y., Xu, R. K., Li, J. Y., and Deng, K. Y.: Phosphate-induced aggregation kinetics of hematite and goethite nanoparticles, J. Soils Sediments, 17, 352–363, 2017.

Xu, C. Y., Zhou, T. T., Wang, C. L., Liu, H. Y., Zhang, C. T., Hu, F. N., Zhao, S. W., and Geng, Z. C.: Aggregation of polydisperse soil colloidal particles: Dependence of Hamaker constant on particle size, Geoderma, 359, 113999, https://doi.org/10.1016/j.geoderma.2019.113999, 2020b.

Xu, Z., Pan, D. Q., Sun, Y. L., and Wu, W. S.: Stability of GMZ bentonite colloids: Aggregation kinetic and reversibility study, Appl. Clay Sci., 161, 436–443, 2018.

Yin, X. Q., Gao, B., Ma, L. Q., Saha, U. K., Sun, H. M., and Wang, G. D.: Colloid-facilitated Pb transport in two shooting-range soils in Florida, J. Hazard. Mater., 177, 620–625, 2010.

Yu, X., Fu, Y., and Lu, S.: Characterization of the pore structure and cementing substances of soil aggregates by a combination of synchrotron radiation X-ray micro–computed tomography and scanning electron microscopy, Eur. J. Soil Sci., 68, 66–79, 2017.

Zhang, Q., Bol, R., Amelung, W., Missong, A., Siemens, J., and Mülder, I.: Water dispersible colloids and related nutrient availability in Amazonian Terra Preta soils, Geoderma, 397, 115103, https://doi.org/10.1016/j.geoderma.2021.115103, 2021.

Zhang, Z. Y., Huang, L., Liu, F., Wang, M. K., Fu, Q. L., and Zhu, J.: Characteristics of clay minerals in soil particles of two Alfisols in China, Appl. Clay Sci., 120, 51–60, 2016.

Zhou, D. X., Ji, Z. X., Jiang, X. M., Dunphy, D. R., Brinker, J., and Keller A. A.: Influence of material properties on TiO_2 nanoparticle agglomeration, PLoS One, 8, e81239, https://doi.org/10.1371/journal.pone.0081239, 2013.

Zhu, X., Chen, H., Li, W., He, Y., Brookes, P. C., and Xu, J.: Aggregation kinetics of natural soil nanoparticles in different electrolytes, Eur. J. Soil Sci., 65, 206–217, 2014.